基于扫描隧道显微镜的单原子自旋共振技术

杨 锴[1*] Andreas Heinrich[2,3] Christopher Lutz[4]
（1. 中国科学院物理研究所 北京 100190；
2. 韩国基础科学研究院量子纳米科学中心 首尔 03760；
3. 韩国梨花女子大学物理系 首尔 03760；
4. 美国IBM Almaden研究中心 圣何塞 95120）

Single-Atom Spin Resonance in a Scanning Tunneling Microscope

YANG Kai[1*], HEINRICH Andreas[2,3], LUTZ Christopher[4]
(1. *Institute of Physics, Chinese Academy of Sciences, Beijing* 100190, *China*;
2. *Center for Quantum Nanoscience, Institute for Basic Science (IBS), Seoul 03760, Republic of Korea*;
3. *Department of Physics, Ewha Womans University, Seoul 03760, Republic of Korea*;
4. *IBM Almaden Research Center, San Jose, CA* 95120, *USA*)

Abstract Recently, the ability to drive electron spin resonance (ESR) of individual atoms using a scanning tunneling microscope (STM) provided a major step forward in sensing and manipulating magnetism at the atomic scale. The atomic-scale spatial resolution and the ultrahigh energy resolution of ESR-STM has allowed the measurement of the magnetic dipolar interaction between two atoms placed a few nanometers apart on a surface, the detection of hyperfine interaction between electronic and nuclear spins of individual atoms, as well as the exploration of quantum fluctuations in designed spin arrays having tailored geometries. By implementing pulsed ESR, coherent spin manipulation of magnetic atoms and engineered atomic dimers on surfaces have been achieved by demonstrating Rabi oscillations, Ramsey fringes and spin echoes, opening the door to a powerful suite of pulsed techniques that can extend single-atom sensing capabilities. Coherent control of spins arranged with atomic precision provides a solid-state platform for quantum simulation of many-body systems.

Keywords Scanning tunneling microscopy, Electron spin resonance, Magnetic atoms, Quantum sensing, Quantum simulations

摘要 近年来，应用扫描隧道显微镜技术已经可以测量单个原子的电子自旋共振谱线，为实现原子尺度量子磁性的探测与操控迈出了重要一步。电子自旋共振扫描隧道显微镜具有原子分辨能力和几十个纳电子伏的超高能量分辨率，可以实现微弱信号的原子尺度探测，例如可以测量固体表面相距几纳米的两个原子之间的微弱磁偶极相互作用、单个原子的电子与核自旋之间的超精细相互作用，以及人工自旋阵列的量子涨落等。借助脉冲式电子自旋共振技术，可以进一步实现固体表面单个磁性原子以及耦合原子的量子相干操控，测量其拉比振荡、拉姆齐干涉条纹和自旋回波信号等。单原子脉冲式电子自旋共振的实现为应用单原子量子探针进行量子探测奠定了重要基础。另外，对具有原子级精度的人工自旋结构的量子相干操控，为多体系统的量子模拟提供了重要的固态实验平台。

关键词 扫描隧道显微镜 电子自旋共振 磁性原子 量子探测 量子模拟
中图分类号：O4-34 **文献标识码**：A **doi**：10. 13922/j. cnki. cjvst. 202107007

Electron spin resonance (ESR), also known as electron paramagnetic resonance (EPR), is a spectroscopic method for investigating paramagnetic substances in liquids and solids[1-2]. These paramagnetic substances

收稿日期：2021-07-13
基金项目：国家自然科学基金委项目(12174433)；中国科学院物理研究所人才计划；Institute for Basic Science (IBS-R027-D1)
* **联系人**：Tel：(010)82648095；E-mail：kaiyang@iphy.ac.cn

commonly possess free radicals, transition metals ions, or paramagnetic defects. By illuminating the samples with electromagnetic radiation at microwave frequencies, ESR spectroscopy has been widely used for studying metal complexes, organic radicals, catalysts and biological samples. A unique advantage of ESR spectroscopy is the ability to reveal the local electronic and magnetic environment of the paramagnetic centers, which can provide valuable insight into solid-state dynamics, phase transitions and even exotic quantum states such as quantum spin liquids[1-3].

Conventional ESR spectroscopy requires a large ensemble (~10^7 to 10^{10} spins) of electron spins to achieve a high enough signal-to-noise ratio[1-2]. Furthermore, ensemble measurements suffer from inhomogeneous broadening–the result of averaging over many non-identical spins–which can mask some of the important physical phenomenon associated with individual spins. The need for a large ensemble also limits the application of ESR in the context of miniaturization of storage and electronic devices, especially for investigating individual atomic-scale magnetic nanostructures for novel data storage, spintronic devices, and quantum computing applications[4-9].

Over the last two decades, ESR spectroscopy has been combined with different scanning probe techniques and semiconductor electronic devices to address the quantum spins at the single atom or single molecule scale[9-11]. For example, coherent control of single spins using ESR has been performed on quantum dots, dopants in semiconductors, nitrogen-vacancy centers in diamond, as well as in magnetic force microscopy[6-10].

A promising new avenue to improve the spatial resolution of ESR measurements is the use of scanning tunneling microscopy (STM), which is capable of constructing and imaging atomic-scale structures, as well as probing spin-spin interactions[12-13], spin dynamics[14-16] and tracking single-molecule motion[17-18]. Notably, artificial nanostructures built by STM have developed into a fruitful testing ground for exploring quantum magnetism[13,16,19-21].

Combing ESR and STM greatly improves the energy resolution of STM and offers a new level of quantum control of spin systems at the atomic level. The idea of combing ESR and STM dates to the 1990s, when the effort was focused on the detection of increased noise in the tunneling current at the spin precession frequency[22-24], but the presence of a frequency-dependent current signal has been sporadic[25]. In 2015, Baumann et al. at the IBM Almaden Research Center reported the successful marriage of ESR techniques to spin-polarized STM, by detecting the ESR of individual Fe atoms adsorbed on a thin MgO film grown on Ag(001)[26].

The use of ESR in STM has outstanding advantages over conventional tunneling spectroscopy used in STM. First, the demonstrated energy resolution of ESR-STM is about 10 neV, which is more than 1000 times better than conventional STM spectroscopy, such as inelastic electron tunneling spectroscopy, which is intrinsically thermally limited[27]. Second, the ESR-STM gives access to the phase information of the quantum states and allows the coherent control of the quantum states by generating quantum superpositions and entanglement with exquisite precision[28].

In this survey, we summarize the recent development and applications of ESR-STM. We start by briefly describing the basic principles of ESR (Section 1) and the implementation of radio-frequency (RF) circuits in a low-temperature STM, in particular the characterization of the transfer function from the RF voltage source to the STM tunnel junction (Section 2). We then focus on the driving and detection mechanism of ESR-STM of magnetic atoms in Section 3, and discuss the important roles of the magnetic tip. In Section 4, we present several applications of ESR-STM techniques on atomic-scale magnetic nanostructures, including quantum sensing, quantum computing and quantum simulation, and both continuous-wave ESR and pulsed ESR will be discussed. Finally, some future directions and challenges will be mentioned.

1 Basic principles of ESR

The basic principle of ESR is as follows[2]. Consider a particle with spin S = 1/2 in an externally

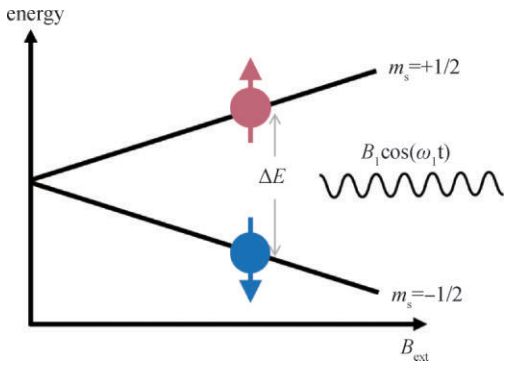

图1　电子自旋共振的基本原理。当一个交变磁场的频率与自旋塞曼能匹配时,可引起电子自旋共振

Fig.1　Basic principles of ESR. An oscillating magnetic field drives an ESR transition between spin up and spin down states when its frequency matches the Zeeman energy determined by the applied magnetic field

applied magnetic field B_{ext}. The spin Hamiltonian describing the Zeeman interaction is

$$H = \gamma\hbar B_{ext} S_z \tag{1}$$

Here γ is the gyromagnetic ratio, $\hbar$ is the reduced Plank constant, and the external field is chosen to point along the z axis. The spin up and spin down states are thus separated by an energy spacing $\Delta E = \gamma\hbar B_{ext}$. To drive the spin resonance, an alternating magnetic field is applied along an axis perpendicular to the static external field. The corresponding perturbing term in the Hamiltonian is

$$H_1 = \gamma\hbar B_1 S_x \cos\omega t \tag{2}$$

When the frequency of the oscillating magnetic field matches the frequency of the Larmor precession of the spin, i. e. $\omega = \gamma B_{ext}$, transitions between the spin up and spin down occur even for $B_1 \ll B_{ext}$. The coherent oscillation of spin is called the Rabi oscillation.

2　Implementing RF circuit in STM

The Zeeman energy of an electron spin is about 28 GHz at a magnetic field of 1 T. Thus, in order to drive ESR of atomic spins using STM, GHz-frequency signals need to be introduced into the tunnel junction. High-frequency electric fields can be applied to the STM tunnel junction by directly applying an RF voltage to the STM tip through a coaxial cable (Fig. 2(a))[26,29-32], or by capacitively inducing an RF electric field across the tunnel junction using a coaxial antenna nearby (Fig. 2(b))[33-34]. Both methods have been successfully employed to drive ESR of surface spins[26,29-34]. In comparison, a high-frequency magnetic field is technically difficult to create in a low-temperature STM junction due to potential heating problems. Even though the RF electric field doesn't directly couple to the atomic spins, the large voltages attainable in the tunnel junction can induce an effective RF magnetic field that is essential to drive ESR, details of which will be discussed in Section 3.

During the ESR-STM measurement, it is desirable to sweep the RF frequency, instead of the magnitude of the static magnetic field, to avoid vibration and heating[35]. Changing the external magnetic field could also lead to a change of quantum states of spin systems. Thus, it is critical to characterize the transfer function from the RF voltage source to the STM junction and to compensate for the cabling resonances and attenuations at each frequency. Without a careful measure of the transfer function, the cabling resonance peaks could easily be misinterpreted for spin resonances. In the following, we briefly discuss the compensation procedure, and the details can be found in ref. [35].

To measure the RF voltage V_{RF} at the tunnel junction, the key idea is to use the nonlinearity in the I-V curve to rectify the RF voltage and convert it to a time-averaged DC tunneling current. For an ideal piecewise linear I-V curve, as shown in Fig. 2(c), the change of the tunneling current ΔI due to the RF voltage is proportional to V_{RF}, and ΔI can be measured by a chopping scheme using a lock-in amplifier[26,35]. In practice, the I-V nonlinearity is available, for example, from the spin excitation of single Fe or Co atoms on MgO layers, observed as a sharp step in the dI/dV curve (Fig. 2(d)). The transfer function is calculated as the ratio of the measured V_{RF} and the RF amplitude of the source V_{Src} (Fig. 2(e))

$$H(f) = \frac{V_{RF}(f)}{V_{Src}} \tag{3}$$

This frequency-dependent transfer function can be verified by creating a frequency sweep with variable power at the RF source proportional to $1/H(f)$, which

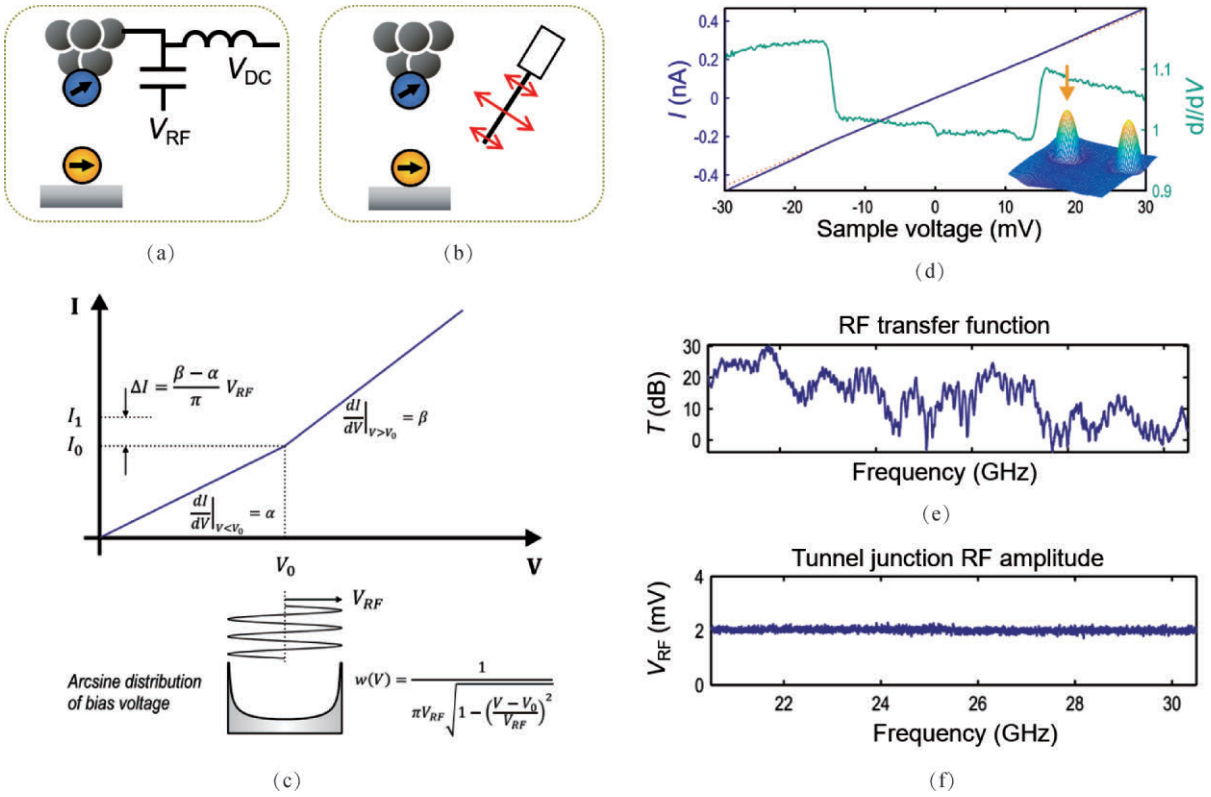

图2 STM中ESR测量的实现。(a),(b) 两种将射频信号引入到STM隧道结的方式的示意图。(c) 分段线性的*I-V*曲线对射频电压的整流效应[35]。(d) 吸附在MgO薄膜表面的单个Fe原子的*I-V*和d*I*/d*V*谱线[35]。(e) 20.5–30.5 GHz范围内的射频传输函数[35]。(f) 按照射频传输函数进行频率扫描来验证射频传输函数[35]

Fig.2 Implementation of ESR in STM. (a),(b) Schematic of the two methods of introducing RF signals into the STM tunneling junction. (c) Rectification of the RF voltage by a piecewise linear *I-V* curve[35]. (d) *I-V* and conductance d*I*/d*V* for Fe atoms on a thin MgO layer[35]. (e) RF transfer function in the range of 20.5–30.5 GHz[35]. (f) Verification of the RF transfer function by creating a frequency sweep with variable power at the RF source according to the transfer function[35]. (c)–(f) Reproduced with permission from Ref [35]. Copyright 2016, American Institute of Physics

results in a constant RF amplitude at the junction. Figure 2(g) indicates that $H(f)$ has been accurately characterized and compensated, so the required frequency-independent RF voltage is generated at the tunnel junction.

3 Driving and detection mechanism of ESR-STM

ESR of single atoms have been measured on magnetic atoms with different atomic spins by using spin-polarized STM tips to probe Fe (spin S=2), hydrogenated Ti (spin S=1/2, referred to as Ti in the following for simplicity), and Cu (spin S=1/2) on two-monolayer MgO[26,36-37]. We have discussed the method to introduce well-characterized RF voltage to the STM junction. However, the RF electric field due to V_{RF} does not couple to the surface spins directly. To drive ESR of atomic spins, the RF electric field needs to induce a RF magnetic field oscillating at the Larmor frequency. The origin of the RF magnetic field cannot be the oscillating tunneling current or the displacement current induced by V_{RF}, as the corresponding magnetic field is too small to account for the measured Rabi frequencies[38].

3.1 Driving mechanism of ESR in STM

Several driving mechanisms of ESR of magnetic atoms have been proposed, including the modulation of any of several junction properties: the magnetic interaction between tip and surface atom[38-40], the ligand field[26], the tunnel junction transmission[41], the adatom's *g*-factor anisotropy[42], and the spin torque due to the tunneling electrons[43]. Among these pro-

posed mechanisms, only the magnetic interaction modulation mechanism is consistent with the measured Rabi frequency being exponential in the tip-to-adatom distance, and insensitive to the tunnel current at a given tip height[28,38,40]. We describe the exchange modulation mechanism in the following by using the ESR of spin 1/2 Ti atoms on MgO as an example.

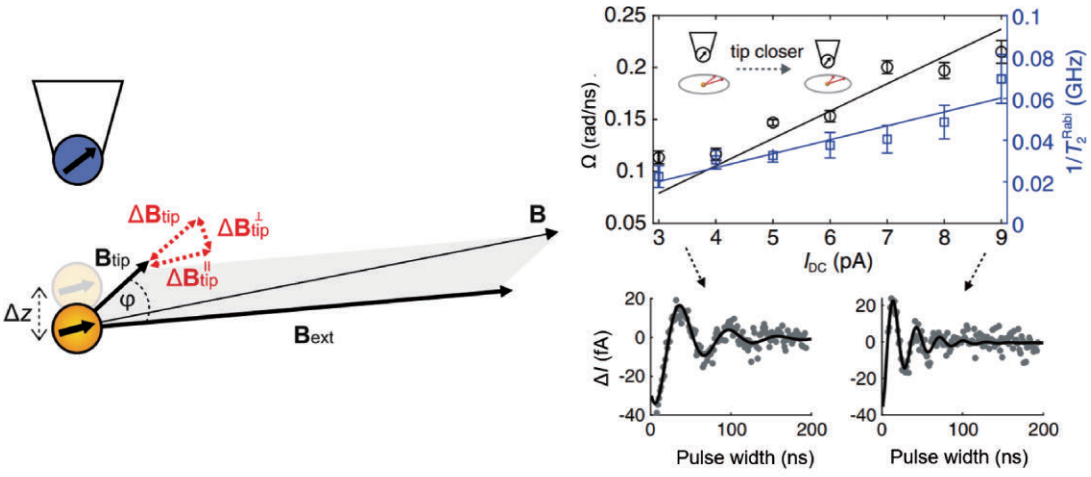

(a)　　(b)

图3　ESR的驱动机制。(a)一种调制针尖与Ti原子之间的磁性相互作用的ESR机制[38]。(b)拉比频率和去相干时间随电流设定值I_{DC}的变化。测量时偏压为50 mV。下图为分别在I_{DC} = 3 pA 和9 pA时的拉比振荡[28]

Fig.3　ESR driving mechanism. (a) Schematic of one possible ESR driving mechanism involving the modulation of tip-Ti magnetic interactions. (b) Rabi frequencies and coherence times at different tip-Ti distances set by different setpoint current I_{DC} at a bias voltage of 50 mV. Lower panels show the Rabi oscillation with fitting at I_{DC} = 3 pA and 9 pA. (a) Reproduced with permission from Ref [38]. Copyright 2019, American Physical Society. (b) Reproduced with permission from Ref [28]. Copyright 2019, American Association for the Advancement of Science (AAAS)

In an ESR-STM measurement, a spin-polarized tip is positioned above a Ti atom (Fig. 3(a)). The spin-polarized tip is made by transferring several Fe atoms from the surface to the tip apex. The Fe atoms at the tip apex interact with the surface Ti atoms via exchange interaction at a typical tip-atom distance of ~ 0.4 nm[38,44], resulting in an effective tip magnetic field B_{tip}. The mechanism is that the RF electric field induces a small displacement of the Ti atom by a piezoelectric effect. Since B_{tip} is strongly spatially inhomogeneous, the vertical displacement Δz results in an oscillating magnetic field with a component that is perpendicular to the total field applied on the Ti atom (Fig. 3(a)). The amplitude of the driving field $\Delta B_{tip}^{\perp}$ is related to the displacement Δz at tip-Ti distance z by

$$\Delta B_{tip}^{\perp}(z) = \frac{\partial B_{tip}}{\partial z}\Delta z \sin\varphi \propto \frac{\exp\left(-z/d_{exch}\right)}{z} \quad (4)$$

where φ is the angle between the tip field and the external magnetic field, and d_{exch} is the decay length of the exchange interaction between the tip and the Ti atom. Both φ and d_{exch} can be obtained by measuring the z-dependent ESR frequencies, allowing for a quantitative calculation of the oscillating magnetic field[38]. The Rabi frequency, which is proportional to $\Delta B_{tip}^{\perp}$, thus has the same exponential dependence on z as the exchange coupling. This exponential dependence has been experimentally verified for Ti atoms on MgO (Fig. 3(b))[28,38,40]. Note that for larger tip-atom distance, the oscillating magnetic field could also have a contribution from the magnetic dipolar interaction between the tip and surface atoms, as shown for the Fe atoms on MgO in a recent work[40].

3.2　DC and homodyne detection of ESR signals

As shown above, the Rabi frequency is nonzero as long as the tip field and external magnetic field are not aligned. The direction of the tip magnetic field is

not only essential for driving ESR, but also important for determining the ESR detection channels of magnetic atoms. The detection of the ESR signals relies on the tunneling magnetoresistance of the tip-atom junction[45]. Two detection channels are involved including DC and homodyne channels[36,46]. In DC detection, the change of time-average population of spin states is detected by the tip magnetization along the quantization of the surface spin[26]. Homodyne detection depends on the spin polarization of the magnetic tip being canted with respect to the quantization axis of the surface spin; in this case, the Larmor precession of the spin yields an RF conductance at the driving frequency. The RF conductance can then be detected by measuring the time-average current due to V_{RF}, giving homodyne detection[36,46].

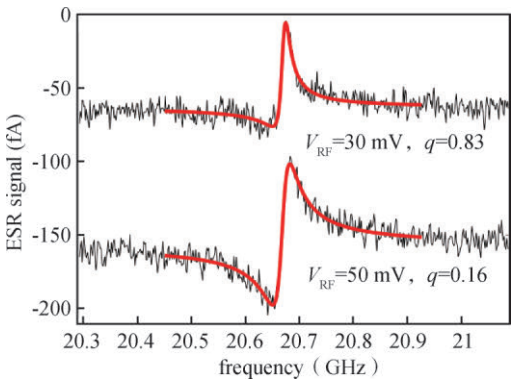

图4 吸附在MgO表面的单个Ti原子的ESR谱线。两条谱线在不同射频电压下测得。红色非对称洛伦兹曲线为利用公式(5)得到的拟合曲线(V_{DC} = 50 mV, I_{DC} = 5 pA, V_{RF} = 30 mV and 50 mV, B_{ext} = 0.82 T)

Fig.4 ESR spectra of a single Ti atom on MgO measured at different RF voltages, and fitted to an asymmetric Lorentzian using equation (5) (V_{DC} = 50 mV, I_{DC} = 5 pA, V_{RF} = 30 mV and 50 mV, B_{ext} = 0.82 T)

The detected current signal during ESR measurement can be described by the steady-state solution to the Bloch equations[46]

$$I_{ESR} = I_0 + I_{sat} \cdot \frac{\Omega^2 T_1 T_2}{1 + \Omega^2 T_1 T_2} \cdot \left(1 + \beta \sin\varphi\right) \cdot \frac{1 + q\delta}{1 + \delta^2} \quad (5)$$

where I_0 is the current far from resonance; I_{sat} is the saturation current; Ω is the Rabi frequency; T_1 is the spin relaxation time; T_2 is the decoherence time; β and q are the asymmetry factors related to homodyne detection; φ accounts for the phase difference between the applied RF voltage and the precession of the Ti spin in the lab frame; $\delta = (f - f_0)/(\Gamma/2)$ is the normalized frequency, and Γ is full width at half-maximum. If the homodyne detection is inactive ($q = 0$), the expression in eq. (5) describes a symmetric Lorentzian lineshape. Homodyne contributes both symmetric and asymmetric components. The relative contribution of the two ESR detection channels is thus reflected in the degree of symmetry of the ESR line shape. For example, the line shape becomes more asymmetric with increasing RF voltage, as homodyne contributes more strongly (Fig. (4)).

4 ESR-STM studies of atomic spin systems

In this section, we present several applications of ESR-STM techniques to studying atomic-scale magnetism, including quantum sensing, quantum computing and quantum simulation.

4.1 Quantum sensing

ESR-STM allows for the detection of magnetic dipolar and exchange interactions between individual atoms on surfaces with the high energy resolution of ESR[36,47-48]. By measuring the spin interaction between an ESR sensor atom and a nearby spin center, one can obtain the magnetic moment of the nearby spin[36,47-48], making ESR-STM a potentially useful tool for quantum sensing of complex magnetic structures such as spin-labelled biomolecules. Compared to other quantum sensors such as the nitrogen-vacancy center in diamond, which has ~10-nm resolution[49], the spatial resolution of this ESR-STM sensor achieves the single atom scale.

· Detecting the magnetic interactions between two individual atoms

The magnetic dipolar coupling between two Fe atoms placed a few nanometers apart on a thin MgO film yields a precise measure of the magnetic moment the Fe atoms (Fig. 5(a)). The Fe under the STM tip is the spin-resonant "sensor" atom, and the other one is the "target" atom. Fe atoms on MgO have a spin S = 2 and strong easy-axis magnetic anisotropy[50], resulting in an effective two-level spin system $|0\rangle$ and $|1\rangle$ that have an expectation value of the spin along the surface

normal $\langle S_z \rangle \approx \pm 2$. ESR measured on the sensor atom shows two peaks (Fig. 5(b)), corresponding to the $|0\rangle$ and $|1\rangle$ states of the target Fe (Fig. 5(c))[47]. The ESR frequency difference gives the magnetic coupling strength, which shows an inverse-cube distance dependence, demonstrating that the Fe atoms are predominantly coupled by dipolar interaction at distances larger than 1 nm. The measured dipolar interaction was used to extract the magnetic moment the Fe atom, yielding 5.44 μ_B (μ_B is the Bohr magneton), in agreement with previous modelling results[47].

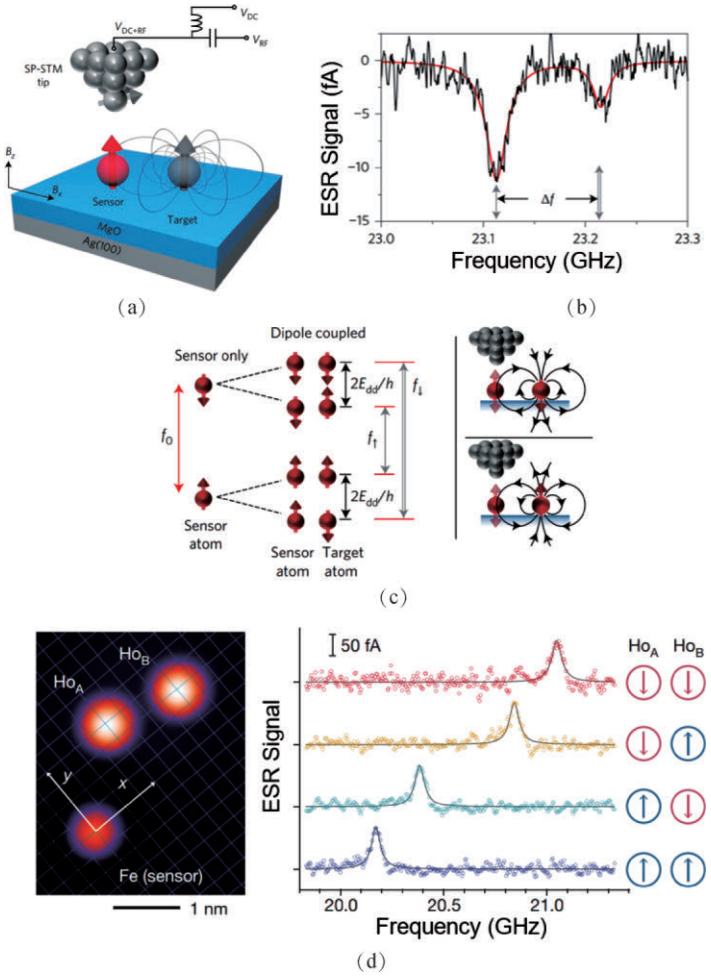

图5　高自旋原子的磁偶极磁场的测量。(a) 测量传感器原子和目标原子之间的磁偶极相互作用的示意图[47]。(b) MgO表面单个Fe原子的ESR谱线,该Fe原子的2.46 nm处放置有另一个Fe原子[47]。(c) 传感器原子和目标原子之间的磁偶极相互作用导致的能级变化[47]。(d) 一个由两个Ho原子构成的双比特存储器,其状态可由附近Fe传感原子处的ESR谱线测得[48]

Fig.5　Detecting atomic dipolar magnetic fields of large-spin atoms. (a) Schematic for sensing the magnetic dipolar interaction between a sensor atom and a target atom. (b) ESR spectrum of an Fe atom on MgO when another Fe atom is positioned 2.46 nm away. (c) Schematic of the energy levels of the sensor atom, modified by the dipolar interaction with the target. (d) A stable two-bit atomic Ho array and the ESR spectra demonstrating state read-out as measured on the Fe sensor atom. (a)-(c) Reproduced with permission from Ref[47]. Copyright 2017, Springer Nature. (d) Reproduced with permission from Ref [48]. Copyright 2017, Springer Nature

The precise measure of the magnetic moment of Fe atoms can be used to sense other atoms such as the bistable magnetic bits formed by individual Ho atoms on MgO, which shows that Ho has a large out-of-plane moment of 10.1 ± 0.1 μ_B on MgO[48]. By monitoring the ESR peak position of Fe, one can remotely read out

the spin states of Ho, which displays a lifetime of many hours at 4 K in an applied magnetic field. In addition, current pulses were used to reversibly switch the magnetic state of Ho. To demonstrate independent reading and writing, an atomic-scale structure with two Ho atomic bits was built, and four possible states were read out remotely by ESR of an Fe sensor (Fig. 5(d))[48], demonstrating that single-atom magnetic memory is indeed possible.

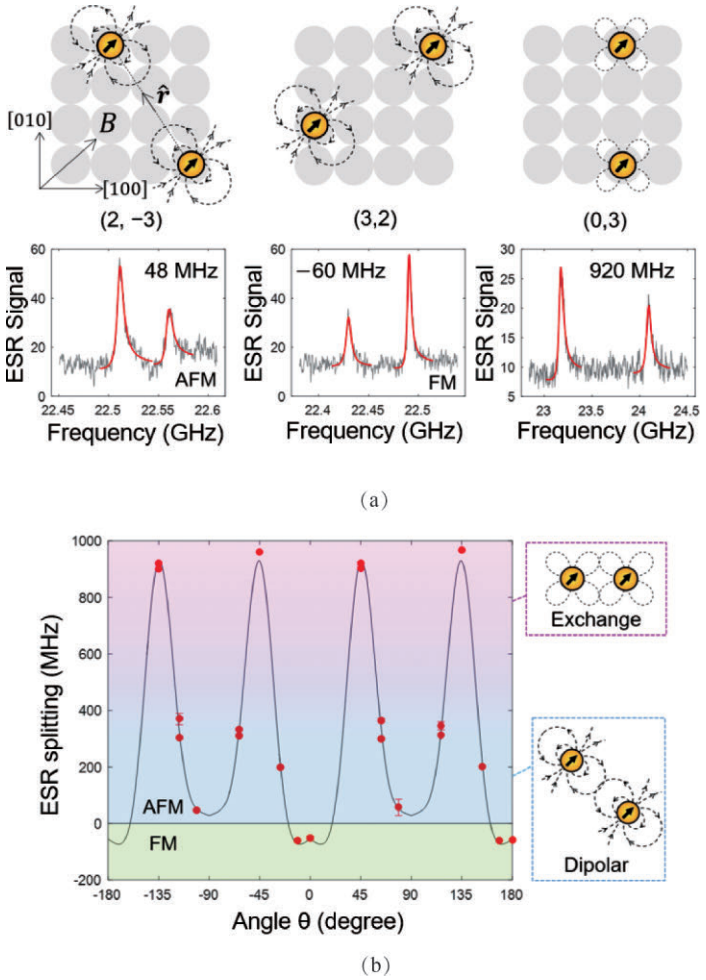

图6 自旋为1/2的Ti原子之间的磁性耦合作用。(a) MgO表面构筑的Ti原子对的位置示意图,以及相应的ESR谱线[36]。(b) 11个相对面内磁场有不同取向的Ti原子对的ESR峰的劈裂大小[36]

Fig.6 Magnetic couplings between two spin−1/2 Ti atoms. (a) Positions of assembled Ti dimers on the oxygen sites of MgO thin film, and the corresponding ESR spectra. (b) ESR splitting of 11 assembled Ti dimers at different orientations with respect to the in-plane magnetic field, fit using the dipole and exchange model. (a)−(b) Reproduced with permission from Ref[36]. Copyright 2017, American Physical Society

Both Fe and Ho atoms are large-spin systems with strong magnetic anisotropy, resulting in Ising-like interactions. In contrast, Ti atoms on MgO reveal spin-1/2 behavior with negligible magnetic anisotropy, and thus quantum fluctuations are maximal[36,46], yielding intriguing quantum superposition phenomena[36,46,51]. The spin Hamiltonian $H = H_{\mathrm{Zee}} + H_{\mathrm{int}}$ describing the spin interactions of two Ti adatoms consists of two parts

$$H_{\mathrm{Zee}} = \gamma\hbar S_{1z}\left(B_{\mathrm{ext}} + B_{\mathrm{tip}}\right) + \gamma\hbar S_{2z}B_{\mathrm{ext}} \quad (6)$$

$$H_{\mathrm{int}} = J\,\boldsymbol{S}_1 \cdot \boldsymbol{S}_2 + D\left(3S_{1z}S_{2z} - \boldsymbol{S}_1 \cdot \boldsymbol{S}_2\right) \quad (7)$$

Here H_{Zee} represents the Zeeman energy, where $\boldsymbol{S}_i = (S_{ix}, S_{iy}, S_{iz})$ is the spin operator of atom i, and γ is the gyromagnetic ratio. The direction of the externally applied magnetic field B_{ext} is defined as z. The Ti spin

under the tip (S_1) experiences an additional tip magnetic field (B_{tip}). The interaction Hamiltonian H_{int} describes the both the exchange (J) and dipolar (D) couplings between the two Ti spins. The J and D can be controlled by adjusting the relative spatial positions of the two Ti spins using STM manipulation, and the splitting between the ESR peaks $\Delta f = (J + 2D)/\hbar$ offers a precise measure of the magnetic interaction strength, which strongly depends on the relative spatial positions of the atoms (Fig. (6))[36].

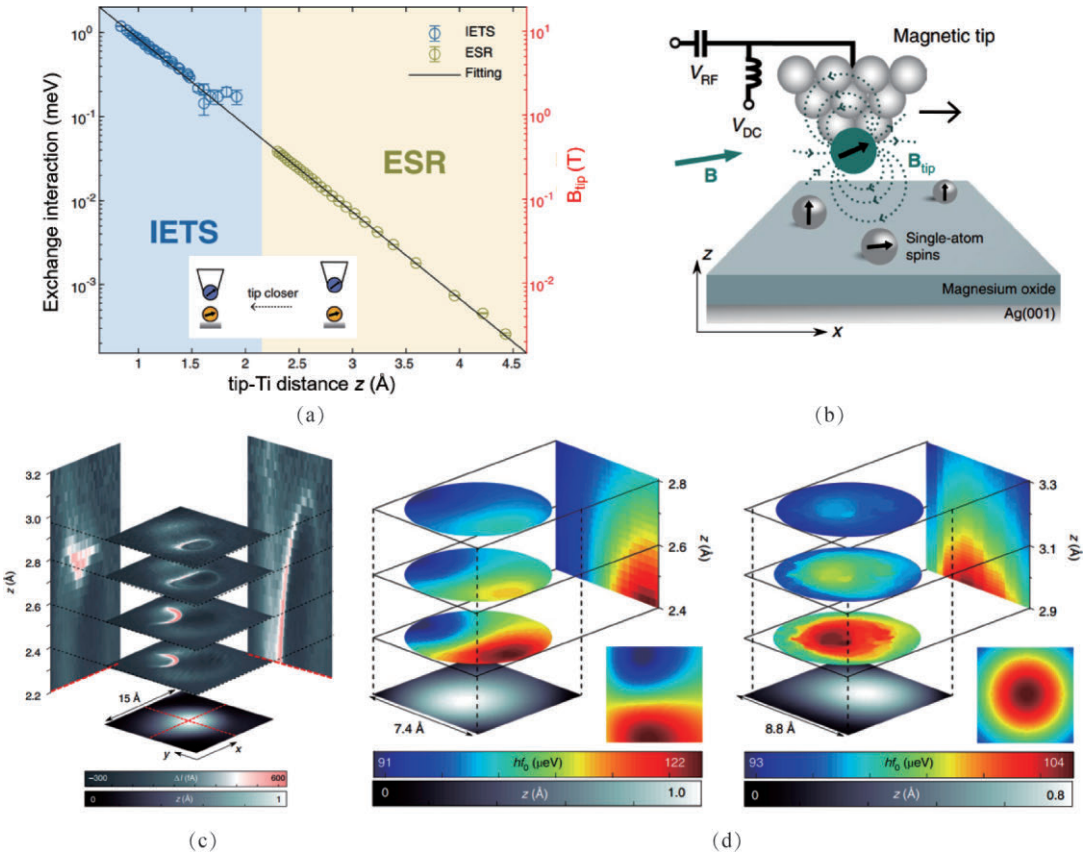

图7　针尖与吸附原子之间的相互作用。(a) MgO 表面的单个 Ti 原子与磁性针尖的交换相互作用随针尖-原子距离的变化[38]。(b) 应用磁性针尖对表面原子进行磁共振成像的示意图[44]。(c) 在不同针尖高度下测得的磁共振成像切面图[44]。(d) 在三维空间中测量磁偶极和交换相互作用两种磁性作用的大小[44]

Fig.7　Tip-adatom interaction. (a) Exchange interaction between a magnetic tip and a Ti atom on MgO as a function of tip-to-atom distance. (b) Schematic of the MRI of single atoms on surface using a magnetic tip. (c) MRI resonant slices imaged at different tip heights. (d) Mapping the 3D magnetic interaction potential, including the dipolar and exchange interaction. (a) Reproduced with permission from Ref[38]. Copyright 2019, American Physical Society. (b)-(d) Reproduced with permission from Ref[44]. Copyright 2019, Springer Nature

The precise characterization of the magnetic properties of spin-polarized STM tip is normally difficult to perform. Using a well-defined magnetic adatom as the sensor, the tip magnetic field can be continuously tuned and measured from 1 mT to 10 T, by adjusting the separation z between a Ti adatom and the magnetic tip (Fig. 7(a))[38]. The large energy range is achieved by combing ESR with inelastic electron tunneling spectroscopy[27]. This control of tip magnetic field over a wide span of energies provides versatile control of coupled quantum spin states as will be discussed in Section 4.2. In addition, the measured tip magnetic field allows for a direct verification of the exchange modulation mechanism for driving ESR[38].

In addition to varying the tip position in the surface normal direction (z), one can also perform ESR measurement at different positions in the x-y plane, referred to as magnetic resonance imaging (Fig. 7(b)).

One can then obtain 'resonant slice' pattern for ESR mapping at constant frequencies, since the tip magnetic field shifts the Zeeman energy of the surface spin and leads to spatial variations in the resonant frequency (Fig. 7(c)). The resonant slice pattern changes for different tip apexes and for different adatom species, revealing cases where either the exchange or the dipolar interaction is dominant[44]. The full 3D interaction potentials between the tip and the surface spin can be obtained by combining many ESR resonant slices (Fig. 7(d))[44].

· Hyperfine interaction between electron spin and nuclear spin

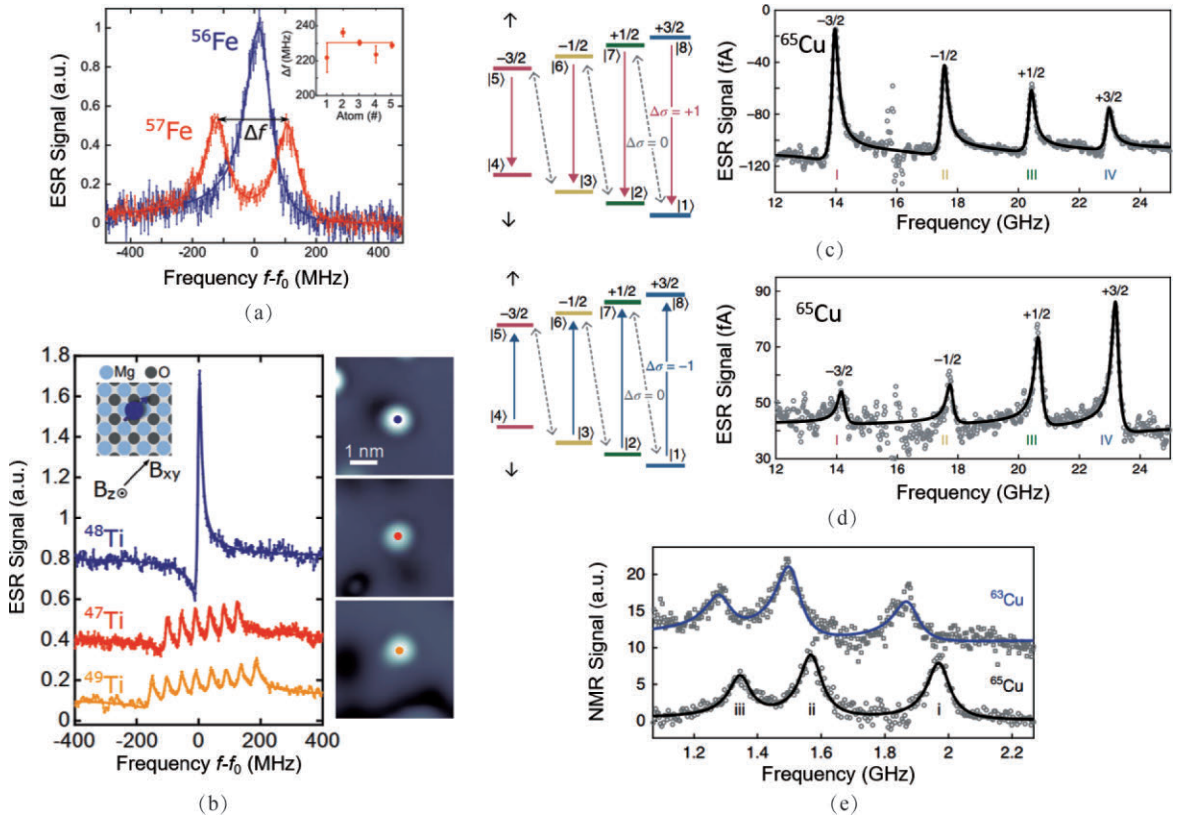

图8 超精细相互作用。(a) MgO表面^{56}Fe和^{57}Fe两种同位素原子的ESR谱线,两种同位素分别具有0和1/2的核自旋[52]。(b) MgO表面^{47}Ti, ^{48}Ti和^{49}Ti三种同位素原子的ESR谱线,三种同位素分别具有5/2, 0和7/2的核自旋[52]。(c),(d) 应用自旋极化电流实现MgO表面单个^{65}Cu原子的核自旋极化,ESR谱线显示不同方向的自旋极化电流可将核自旋极化到不同方向[37]。(e) MgO表面^{63}Cu和^{65}Cu两种同位素原子的核磁共振谱线[37]

Fig.8 Hyperfine coupling. (a) ESR spectra for different Fe isotopes including ^{56}Fe and ^{57}Fe atoms on MgO, with nuclear spin I = 0 and 1/2 respectively. (b) ESR spectra for different Ti isotopes including ^{47}Ti, ^{48}Ti and ^{49}Ti atoms on MgO, with nuclear spin I = 5/2, 0 and 7/2 respectively. (c), (d) ESR spectra of single ^{65}Cu atoms on MgO showing different nuclear spin polarization with different directions of spin-polarized current. Left panels shows the spin-transfer torque mechanism for the nuclear spin polarization. (e) NMR spectra of ^{63}Cu and ^{65}Cu atoms on MgO. (a)–(b) Reproduced with permission from Ref[52]. Copyright 2018, AAAS. (c)–(e) Reproduced with permission from Ref[37]. Copyright 2018, Springer Nature

The sensitivity of ESR-STM can also be employed to measure the hyperfine interaction between the electron spin and the nuclear spin of individual magnetic atoms such as Fe, Ti and Cu atoms on MgO[37,52]. The coupled electron-nuclear system in a magnetic field $\boldsymbol{B}_{\text{ext}}$ can be modelled by using an isotropic hyperfine coupling term and electron Zeeman term

$$H = A\mathbf{S}\cdot\boldsymbol{I} + \gamma_e \boldsymbol{B}_{\text{ext}}\cdot\boldsymbol{S} \tag{8}$$

Here A is the hyperfine constant and γ_e is the electron gyromagnetic ratio. The hyperfine coupling term results in $2I+1$ ESR peaks, and the splitting is proportional to A. For example, ^{57}Fe, ^{47}Ti and ^{46}Ti atoms

show 2, 6 and 8 peaks in the ESR spectra, respectively (Fig. 8(a) and 8(b))[37,52]. Thus, ESR performed on single magnetic atoms provides a way to distinguish different isotopes with different nuclear spin numbers. The hyperfine spectrum of Ti on MgO is sensitive to the distinct binding sites of individual Ti atoms, and thus can be further used to extract position-dependent information about the electronic ground states and the properties of the nuclear spin[52].

Compared to Fe and Ti atoms, Cu atoms have a relatively large hyperfine constant of ~3 GHz, which results in more mixed electron-nuclear quantum states[37]. This state mixing enables the polarization of the Cu nuclear spin by using spin-polarized tunneling current, in which the direction and magnitude of the nuclear polarization is controlled by the direction and magnitude of the current (Fig. 8(c) and 8(d))[37]. The current-controlled nuclear polarization is a consequence of the transfer of spin angular momentum from tunneling electrons to the atom's electronic spin, and from there to its nuclear spin[37]. More importantly, the polarized nuclear spin permits the detection of nuclear magnetic resonance (NMR) of individual Cu atoms, by driving the NMR-type resonant transitions between adjacent nuclear spin states (Fig. 8(e))[37]. The electrically driven nuclear polarization and single-atom NMR should now enable detection of the atomic-scale magnetic environment in nanomagnets such as magnetic molecules.

4.2 Simulating quantum magnetism using spin−1/2 Ti atoms

Artificial nanostructures built by STM such as spin chains and arrays have developed into a fruitful testing ground for exploring quantum magnetism[13,16,19-21]. Magnetic ordering such as magnetic bistability[53-54] and highly entangled states[13,20] have been explored by measuring tunneling spectroscopy[13,55], magnetization curves[56-57] and relaxation times[58] using STM. Extending these techniques to include ESR provides highly improved energy resolution, and offers the unique capability to prepare interesting quantum superposition states using pulsed-ESR[28]. Thus, exploration of atomic-scale quantum magnets with ESR-STM opens a new avenue for simulations of quantum magnetism, for understanding strongly correlated physics, and for quantum information processing.

Artificial quantum magnets on MgO have been constructed by using spin−1/2 Ti atoms and measured by ESR-STM[51]. The coupled Ti spins feature strong quantum fluctuations, and the spin Hamiltonian can be engineered by using STM atom manipulation to set the couplings, and by applying external and tip magnetic fields

$$H = \sum_{i,j} J_{ij}\, \boldsymbol{S}_i \cdot \boldsymbol{S}_j + \sum_i g\mu_B \boldsymbol{B}_{ext} \cdot \boldsymbol{S}_i + g\mu_B \boldsymbol{B}_{tip} \cdot \boldsymbol{S}_n \quad (1)$$

Here $\mathbf{S}_i$ is the spin operator for atom i, with a g-factor $g \approx 1.8$, and μ_B is the Bohr magneton. The atomic-scale tip magnetic field $\boldsymbol{B}_{tip}$ is used both to drive ESR transitions and to tune the quantum states by exerting an exchange bias only on the spin $\boldsymbol{S}_n$ under the tip. Consideration of the recently reported g-factor anisotropy[59] could further improve the accuracy of the spin Hamiltonian.

For a pair of coupled Ti spins, the local tip magnetic field can be used to precisely tailor the superpositions in the eigenstates, tuning them either to the Zeeman product states, or to singlet and triplet states (Fig. 9(a))[36]. The evolution of the energy eigenstates and energy levels were quantitatively studied by measuring the shifts of the ESR frequencies (Fig. 9(b)). By tuning to obtain singlet and triplet states, one can realize a singlet-triplet clock transition that shows a factor-of-ten improvement in the quantum coherence time (Fig. 9(c))[46]. In addition, it was recently shown that the free coherent evolution can be observed by using DC pump-probe spectroscopy, when the coupled spin states are tuned to be the singlet and triplet states (Fig. 9(d))[32].

Using the coupled Ti spin pairs as building blocks, one can construct larger quantum magnets, including odd- and even-length spin chains, spin triangles and spin plaquettes, which allows for the exploration of the quantum fluctuation and their dependence on the geometry of the magnetic structures by measuring their many-body states with atomic resolution[36]. For example, the spin plaquette of four Ti spins exhibits a coherent su-

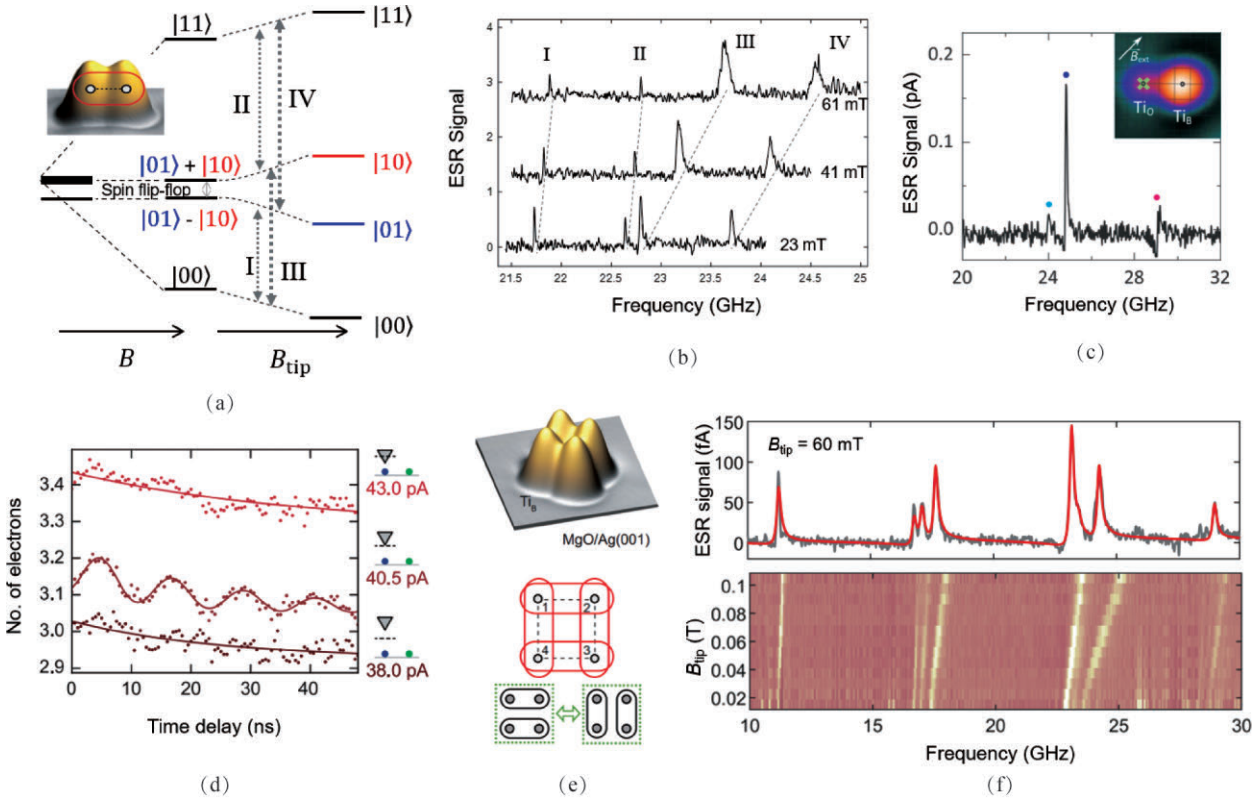

图9 耦合自旋系统的量子态。(a) 两个相互耦合Ti原子自旋的能级随外加磁场和针尖磁场的变化[36]。(b) 在不同针尖磁场下测得的两个相互耦合Ti原子自旋的ESR谱线[36]。(c) 两个相互耦合Ti原子自旋的ESR谱线,其中最高频率峰对应自旋单态–自旋三重态的跃迁[46]。(d) 在不同针尖磁场下对两个相互耦合Ti原子自旋的泵浦测量,中间曲线代表量子态的相干演化[32]。(e) 四个相互耦合的Ti原子的STM图像,以及RVB量子态的示意图[51]。(f) 在不同针尖磁场下测得的四个相互耦合的Ti原子自旋系统的ESR谱线[51]

Fig.9 Quantum states of coupled spins. (a) Schematic energy level diagram of two coupled Ti spins as a function of external and tip magnetic fields. (b) ESR spectra of two coupled Ti spins at different tip magnetic fields. (c) ESR spectrum of two coupled Ti atoms showing the singlet-triplet transition (the peak at the highest frequency). (d) Pump-probe measurements on a coupled Ti dimer at different tip magnetic field, showing the free coherent evolution in the middle curve. (e) STM image of a spin plaquette of Ti atoms and the schematic of the resonating valence bond (RVB) state. (f) ESR spectra measured on one of the four Ti atoms of the spin plaquette at different tip magnetic fields. (a), (b) Reproduced with permission from Ref[36]. Copyright 2018, American Physical Society. (c) Reproduced with permission from Ref[46]. Copyright 2017, AAAS. (d) Reproduced with permission from Ref[32]. Copyright 2021, AAAS. (e), (f) Reproduced with permission from Ref[51]. Copyright 2021, Springer Nature

perposition of spin-singlet pairings, known as the resonating valence bonds (RVB) states (Fig. 9(e)). In such a geometry, there are two valence-bond basis states $|\Phi_=\rangle = (\downarrow_1\uparrow_2 - \uparrow_1\downarrow_2)(\downarrow_4\uparrow_3 - \uparrow_4\downarrow_3)$ and $|\Phi_\parallel\rangle = (\downarrow_1\uparrow_4 - \uparrow_1\downarrow_4)(\downarrow_2\uparrow_3 - \uparrow_2\downarrow_3)$. The RVB state consists of the coherent superposition $|\Phi_=\rangle + |\Phi_\parallel\rangle$, which results in entanglement of each spin with its two neighbors. Direct access to RVB state was obtained by driving an ESR transition into the RVB states, and the relative energy difference between the RVB states and other spin states was then measured from the ESR frequencies to quantify the energy benefit from forming the singlet superpositions (Fig. 9(f))[36].

These designed quantum spin arrays combined with single-atom ESR provide a flexible platform to explore the quantum states of finite-size spin systems, and could be combined with pulsed ESR to further explore the quantum dynamics of quasiparticles with

atomic resolution.

4.3 Coherent manipulation of atomic spins using pulsed ESR

In addition to studying the stationary magnetic states using continuous-wave ESR as shown above, combing pulsed ESR with STM allows for the time-domain control of quantum spin states with atomic-scale resolution[28]. The pulsed ESR is implemented by a pump-probe technique using RF pulses, and the time durations of the pulses are controlled by an external arbitrary waveform generator (Fig. 10(a)). By applying a series of RF pulsed at the resonant frequency on individual Ti atoms on MgO, one can drive the Rabi oscillations between the two spin states, yielding an oscillatory current signal with increasing pulse width (Fig. 10(b)). The Rabi frequency increases monotonically with applied RF voltage, and exponentially with the tip-atom distance[28], reflecting the exchange modulation mechanism discussed in Section 3.

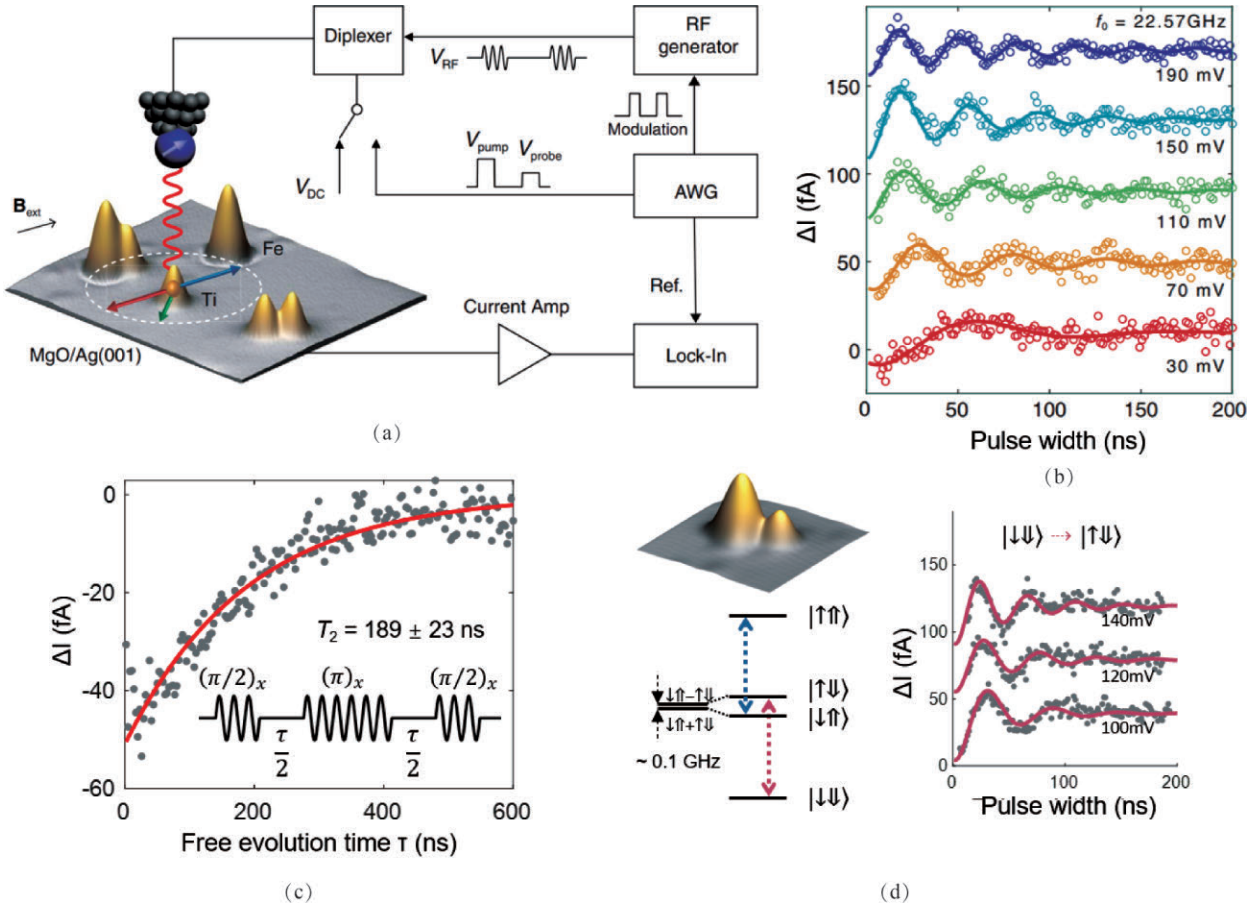

图 10　脉冲式自旋共振。(a) 利用STM实现脉冲式ESR测量的电路示意图[28]。(b) 不同射频电压下测得的MgO表面单个Ti原子自旋的拉比振荡[28]。(c) MgO表面单个Ti原子自旋的自旋回波信号,并由此得到189 ns的去相干时间[28]。(d) MgO表面两个相互作用的Ti原子自旋的STM图像、能级图,及其脉冲式ESR测量[28]

Fig.10　Pulsed spin resonance. (a) Schematic showing the STM circuit for pulsed ESR measurements. (b) Rabi oscillations of a Ti spin on MgO at different RF voltages. (c) Spin-echo signals of a Ti spin on MgO, giving a coherence time of 189 ns. (d) STM image, energy level diagram and pulsed ESR measurement of two coupled Ti spins on MgO. (a)-(d) Reproduced with permission from Ref[28]. Copyright 2021, AAAS

The decay constant of Rabi oscillations gives a coherence time of ~40 ns. The measured coherence time increased to almost 200 ns when performing a Hahn-echo pulse sequence, consisting of a π pulse placed between two π/2 pulses (Fig. 10(c)), indicating that decoherence is caused mainly by slowly varying fields,

such as tip vibration resulting in a slow-varying tip magnetic field[28]. Another main decoherence source is the scattering by electrons in the tunneling current[28,60]. Pulsed ESR can now be employed to extend the sensing capabilities of a single-atom quantum sensors[8-9,11].

Having access to well-characterized spin-resonant atoms at the surface and the ability to build structures with atomic-scale precision offers a unique set of capabilities in the context of solid-state quantum bits. Coherent operations on coupled-spin states in designed atomic structures have been demonstrated by assembling Ti atom pairs at close spacing (Fig. 10(d))[28]. For a weakly coupled spin dimer, one can perform controlled rotation of the target spin under the STM tip, conditionally on the state of the other control spin by selectively driving one of the ESR transitions (Fig. 10(d))[28]. This capability provides a possible realization of the quantum CNOT gate[61]. The coherent control of designed spin structures provides a solid-state platform for quantum simulation of many-body systems.

5 Conclusion and outlook

We have discussed the development of the ESR-STM technique over the last several years, focusing on its applications for the detection of magnetic dipolar and exchange interactions as well as the hyperfine interaction between the nuclear spin and the electron spin. We have also shown that ESR-STM is capable of probing the coupled quantum states such as the RVB states, as well as the fast coherent dynamics of quantum spin states in the time domain by employing the pulsed ESR technique. The combination of STM with ESR thus provides a versatile tool for exploring nanoscale quantum magnetism and for quantum sensing of magnetic nanostructures, with nano-eV energy resolution and a spatial resolution at the single-atom scale.

In addition to investigating atomic spin systems, we expect the quantum sensing capability of the ESR-STM to extend to other systems such as magnetic molecules[62] and low-dimensional condensed matter systems[63], which will greatly advance our ability to probe the quantum magnetism and related strongly-correlated-electron phenomena. We also anticipate that the coherent manipulation of larger spin systems will provide valuable insight into exotic quantum magnetic phases by exploring their quantum states and dynamics[64-65].

参 考 文 献

[1] Slichter C P. Principles of Magnetic Resonance[M]. Springer, 1996

[2] Abragam A, Bleaney B. Electron Paramagnetic Resonance of Transition ions[M]. Oxford University Press, 2012

[3] Miksch B, Pustogow A, Rahim M J, et al. Gapped Magnetic Ground State in Quantum Spin Liquid Candidate κ-(BEDT-TTF)$_2$Cu$_2$(CN)$_3$[J]. Science, 2021, 372(6359): 276-279

[4] Schlauderer S, Lange C, Baierl S, et al. Temporal and Spectral Fingerprints of Ultrafast All-Coherent Spin Switching[J]. Nature, 2019, 569: 383-387

[5] Thiele S, Balestro F, Ballou R, et al. Electrically Driven Nuclear Spin Resonance in Single-Molecule Magnets[J]. Science, 2014, 344(6188): 1135-1138

[6] Nowack K C, Koppens F H L, Nazarov Y V, et al. Coherent Control of a Single Electron Spin with Electric Fields[J]. Science, 2007, 318(5855): 1430-1433

[7] Pla J, Tan K, Dehollain J, et al. A Single-Atom Electron Spin Qubit in Silicon[J]. Nature, 2012, 489: 541-545

[8] Maze J, Stanwix P, Hodges J, et al. Nanoscale Magnetic Sensing with an Individual Electronic Spin in Diamond [J]. Nature, 2008, 455: 644-647

[9] Balasubramanian G, Chan I, Kolesov R, et al. Nanoscale Imaging Magnetometry with Diamond Spins Under Ambient Conditions[J]. Nature, 2008, 455: 648-651

[10] Rugar D, Budakian R, Mamin H D, et al. Single Spin Detection by Magnetic Resonance Force Microscopy[J]. Nature, 2004, 430: 329-332

[11] Degen C L, Reinhard F, Cappellaro P. Quantum Sensing [J]. Rev Mod Phys, 2017, 89: 035002

[12] Czap G, Wagner P J, Xue F, et al. Probing and Imaging Spin Interactions with a Magnetic Single-Molecule Sensor [J]. Science, 2019, 364(6441): 670-673

[13] Hirjibehedin C F, Lutz C P, Heinrich A J. Spin Coupling in Engineered Atomic Structures[J]. Science, 2006, 312(5776): 1021-1024

[14] Loth S, Etzkorn M, Lutz C P, et al. Measurement of Fast Electron Spin Relaxation Times with Atomic Resolution [J]. Science, 2010, 329(5999): 1628-1630

[15] Yoshida S, Aizawa Y, Wang Z, et al. Probing Ultrafast Spin Dynamics with Optical Pump–Probe Scanning Tun-

nelling Microscopy[J]. Nat Nanotechnol, 2014, (9): 588-593

[16] Khajetoorians A A, Baxevanis B, Hübner C, et al. Current-Driven Spin Dynamics of Artificially Constructed Quantum Magnets[J]. Science, 2013,339(6115):55-59

[17] Cocker T, Peller D, Yu P, et al. Tracking the Ultrafast Motion of a Single Molecule by Femtosecond Orbital Imaging[J]. Nature,2016, 539:263-267

[18] Li S, Chen S, Li J, et al. Joint Space-Time Coherent Vibration Driven Conformational Transitions in a Single Molecule[J]. Phys Rev Lett,2017,119:176002

[19] Khajetoorians A, Wiebe J, Chilian B, et al. Atom-By-Atom Engineering and Magnetometry of Tailored Nanomagnets[J]. Nat Phy,2012,(8):497-503

[20] Toskovic R, Berg R V D, Spinelli A, et al. Atomic Spin-Chain Realization of a Model for Quantum Criticality[J]. Nat Phys,2016, 12:656-660

[21] Drost R, Ojanen T, Harju A, et al. Topological States in Engineered Atomic Lattices[J]. Nat Phys, 2017, 13: 668-671

[22] Manassen Y, Hamers R J, Demuth J E, et al. Direct Observation of the Precession of Individual Paramagnetic Spins on Oxidized Silicon Surfaces[J]. Phys Rev Lett, 1989, 62:2531-2534

[23] Manassen Y, Mukhopadhyay I, Rao N R. Electron-Spin-Resonance STM on Iron Atoms in Silicon[J]. Phys Rev B, 2000, 61:16223-16228

[24] Durkan C, Welland M E. Electronic Spin Detection in Molecules Using Scanning-Tunneling- Microscopy-Assisted Electron-Spin Resonance[J]. Appl Phys Lett, 2002, 80:458-460

[25] Balatsky A V, Nishijima M, Manassen Y. Electron Spin Resonance-Scanning Tunneling Microscopy[J]. Adv Phys,2012,61:117-152

[26] Baumann S, Paul W, Choi T, et al. Electron Paramagnetic Resonance of Individual Atoms on a Surface[J]. Science,2015, 350(6259):417-420

[27] Heinrich A J, Gupta J A, Lutz C P, et al. Single-Atom Spin-Flip Spectroscopy[J]. Science, 2004, 306(5695): 466-469

[28] Yang K, Paul W, Phark S H, et al. Coherent Spin Manipulation of Individual Atoms on a Surface[J]. Science, 2019,366(6464): 509-512

[29] Natterer F D, Patthey F, Bilgeri T, et al. Upgrade of a Low-Temperature Scanning Tunneling Microscope for Electron-Spin Resonance[J]. Rev Sci Instrum, 2019, 90: 013706

[30] Willke P, Singhaet A, Zhang X, et al. Tuning Single-Atom Electron Spin Resonance in a Vector Magnetic Field [J]. Nano Lett,2019,19:8201-8206

[31] Van Weerdenburg W M J, Steinbrecher M, Van Mullekom N P E, et al. A Scanning Tunneling Microscope Capable of Electron Spin Resonance and Pump - Probe Spectroscopy at mk Temperature and in Vector Magnetic Field[J]. Rev Sci Instrum,2021,92:033906

[32] Veldman L M, Farinacci L, Rejali R, et al. Free Coherent Evolution of a Coupled Atomic Spin System Initialized by Electron Scattering[J]. Science, 2021, 372 (6545):964-968

[33] Seifert T S, Kovarik S, Nistor C, et al. Single-Atom Electron Paramagnetic Resonance in a Scanning Tunneling Microscope Driven by a Radio-Frequency Antenna at 4 K [J]. Phys Rev Research 2,2020: 013032

[34] Peters O, Bogdanoff N, González S A, et al. Resonant Andreev Reflections Probed by Photon-Assisted Tunnelling at the Atomic Scale[J]. Nat Phys, 2020, 16: 1222-1226

[35] Paul W, Baumann S, Lutz C P, et al. Generation of Constant-Amplitude Radio-Frequency Sweeps at a Tunnel Junction for Spin Resonance STM[J]. Rev Sci Instrum, 2016,87:074703

[36] Yang K, Bae Y, Paul W, et al. Engineering the Eigenstates of Coupled Spin-1/2 Atoms on a Surface[J]. Phys Rev Lett,2017,119:227206

[37] Yang K, Willke P, Bae Y, et al. Electrically Controlled Nuclear Polarization of Individual Atoms[J]. Nat Nanotechnol,2018,13:1120-1125

[38] Yang K, Paul W, Natterer F D, et al. Tuning the Exchange Bias on a Single Atom from 1 mT to 10 T[J]. Phys Rev Lett,2019,122:227203

[39] Lado J L, Ferrón A, Fernández-Rossier J. Exchange Mechanism for Electron Paramagnetic Resonance of Individual Adatoms[J]. Phys Rev B,2017,96:205420

[40] Seifert T S, Kovarik S, Juraschek D M, et al. Longitudinal and Transverse Electron Paramagnetic Resonance in a Scanning Tunneling Microscope[J]. Sci Adv,2020,(6): eabc5511

[41] Gálvez J, Wolf C, Delgado F, et al. Cotunneling Mechanism for All-Electrical Electron Spin Resonance of Single Adsorbed Atoms[J]. Phys Rev B,2019,100:035411

[42] Ferrón A, Rodríguezet S A, Gómez S S, et al. Single Spin Resonance Driven by Electric Modulation of the G-Factor Anisotropy[J]. Phys Rev Research, 2019, (1): 033185

[43] Shakirov A M, Rubtsov A N, Ribeiro P. Spin Transfer Torque Induced Paramagnetic Resonance[J]. Phys Rev B, 2019,99:054434

[44] Willke P, Yang K, Bae Y, et al. Magnetic Resonance Imaging of Single Atoms on a Surface[J]. Nat Phys,2019, 15:1005-1010

[45] Wiesendanger R. Spin Mapping at the Nanoscale and Atomic Scale[J]. Rev Mod Phys,2009,81:1495-1550

[46] Bae Y, Yang K, Willke P, et al. Enhanced Quantum Coherence in Exchange Coupled Spins via Singlet-Triplet Transitions[J]. Sci Adv,2018,4:eaau4159

[47] Choi T, Paul W, Rolf-Pissarczyk S, et al. Atomic-Scale Sensing of the Magnetic Dipolar Field from Single Atoms [J]. Nat Nanotechnol,2017,12:420-424

[48] Natterer F, Yang K, Paul W, et al. Reading and Writing Single-Atom Magnets[J]. Nature,2017,543:226-228

[49] Pelliccione M, Jenkins A, Ovartchaiyapong P, et al. Scanned Probe Imaging of Nanoscale Magnetism at Cryogenic Temperatures with a Single-Spin Quantum Sensor [J]. Nat Nanotechnol,2016,11:700

[50] Paul W, Yang K, Baumann S, et al. Control of the Millisecond Spin Lifetime of an Electrically Probed Atom[J]. Nat Phys,2017,13:403-407

[51] Yang K, Phark S H, Bae Y, et al. Probing Resonating Valence Bond States in Artificial Quantum Magnets[J]. Nat Commun,2021,12:993

[52] Willke P, Bae Y, Yang K, et al. Hyperfine Interaction of Individual Atoms on a Surface[J]. Science, 2018, 362 (6412):336-339

[53] Krause S, Berbil-Bautista L, Herzog G, et al. Current-Induced Magnetization Switching with a Spin-Polarized Scanning Tunneling Microscope[J]. Science, 2007, 317 (5844):1537-1540

[54] Loth S, Baumann S, Lutz C P, et al. Bistability in Atomic-Scale Antiferromagnets[J]. Science,2012,335(6065): 196-199

[55] Bork J, Zhang Y H, Diekhöner L, et al. A Tunable Two-Impurity Kondo System in An Atomic Point Contact[J]. Nat Phys,2011,(7):901-906

[56] Meier F, Zhou L, Wiebe J, et al. Revealing Magnetic Interactions from Single-Atom Magnetization Curves[J]. Science,2008,320(5872):82-86

[57] Khajetoorians A, Wiebe J, Chilian B, et al. Atom-by-Atom Engineering and Magnetometry of Tailored Nanomagnets[J]. Nat Phys,2012,(8):497-503

[58] Yan S, Choi D J, Burgess J, et al. Control of Quantum Magnets by Atomic Exchange Bias[J]. Nat. Nanotechnol, 2015,10: 40-45

[59] Steinbrecher M, Van Weerdenburg W M J, Walraven E F, et al. Quantifying the Interplay Between Fine Structure and Geometry of An Individual Molecule on a Surface [J]. Phys Rev B,2021,103:155405

[60] Willke P, Paul W, Natterer F D, et al. Probing Quantum Coherence in Single-Atom Electron Spin Resonance[J]. Sci. Adv,2018,4, eaaq1543

[61] Gaita-Ariño A, Luis F, Hill S, et al. Molecular Spins for Quantum Computation[J]. Nat Chem, 2019, 11: 301-309

[62] Atzori M, Sessoli R. The Second Quantum Revolution: Role and Challenges of Molecular Chemistry[J]. J Am Chem Soc,2019,141:11339-11352

[63] Geim A K, Grigorieva I V. Van Der Waals Heterostructures[J]. Nature,2013,499:419-425

[64] Choi D J, Lorente N, Wiebe J, et al. Colloquium: Atomic Spin Chains on Surfaces[J]. Rev Mod Phys, 2019, 91, 041001

[65] Khajetoorians A A, Wegner D, Otte A F, et al. Creating Designer Quantum States of Matter Atom-by-Atom[J]. Nat Rev Phys,2019,(1):703-715